THE JOURNAL OF PHYSICAL CHEMISTRY C
A JOURNAL OF THE AMERICAN CHEMICAL SOCIETY

pubs.acs.org/JPCC

Article

Density Functional Theory Investigation of Graphene Functionalization with Activated Carbenes and Its Application in the Sensing of Heavy Metallic Cations

Sabrine Baachaoui, Sarah Aldulaijan, Luca Sementa, Alessandro Fortunelli,* Adnene Dhouib,* and Noureddine Raouafi*

Cite This: *J. Phys. Chem. C* 2021, 125, 26418−26428

Read Online

ACCESS | Metrics & More | Article Recommendations | Supporting Information

ABSTRACT: Anthropogenic activities presently generate undesirable industrial and house waste byproducts such as heavy metallic cations (HMCs), which are then often released into the environment, despite being harmful to human beings. Developing new materials that can detect and capture HMCs is therefore highly desirable for wastewater remediation, especially if using cheap starting raw materials such as carbon. To shed theoretical light in this direction, we use density functional theory simulations to study the functionalization of pristine graphene with prototypical carbenes, RC(O)CH, with R = $-OCH_3$ (**2a**), −OH (**2b**), −ONa (**2c**), and −Ph (**2d**), and explore their use in sensing and capturing toxic HMCs (here, we focus on the most common and harmful ones: Cd^{2+}, Hg^{2+}, and Pb^{2+}). We first demonstrate that, starting from activated diazomethanes, $RC(O)CHN_2$ (**1a−d**), and graphene as precursors, it is possible to yield substituted cyclopropanes tethered to graphene, here modeled as a 6 × 6 supercell (**g6×6**), via a [2 + 1]—cycloaddition reaction. Projected density of states and band structure calculations show that the cycloaddition reaction induces a band gap opening of the graphene, which can be used to tune it for electronic sensing devices. These nanomaterials (**g6×6/3a−d**) favorably interact with the metallic cations through coordination bonds with interaction energies varying from −1.18 to −2.75 eV. Differences in the electronic charge density following HMC adsorption reveal regions of electron depletion or gain induced by these interactions. Based on energetic and electronic structure analysis, we suggest that **g6×6/3b−d** are good candidates to detect HMCs. All the four nanomaterials show a higher affinity toward Pb^{2+}, as rationalized by a synergic interaction with the graphene substrate, suggesting that they can be used for Pb^{2+} sensing and removal. Notably, we demonstrate that once and *only* once the proper computational approach is employed, the accuracy of our predictions of a larger interaction strength of Pb^{2+} with respect to Cd^{2+} is validated via the agreement with available experimental data on **g6×6/3b**. Finally, we predict that by varying the pH, the **g6×6/3b,c** pair can be employed to differentially sense Cd^{2+} and Hg^{2+} cations.

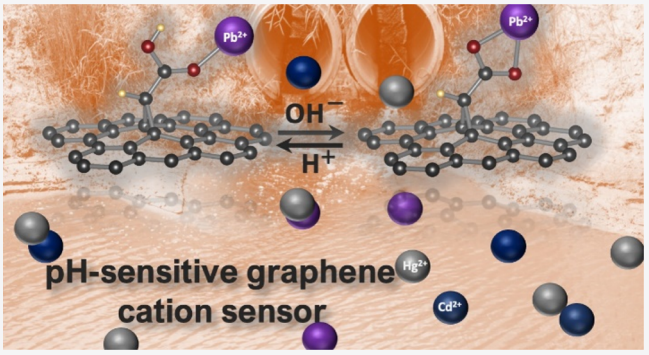

1. INTRODUCTION

Anthropogenic activities produce several by-products in industry and domestic life. Some of them are harmful to humans and can cause serious diseases. The World Health Organization recommends maximum levels of a few parts per billions (ppb) of the most toxic elements.[1] Among the most dangerous wastewater contaminants, heavy metallic cations (HMCs) such as Cd^{2+}, Hg^{2+}, and Pb^{2+} (Cd: 3 ppb, Pb: 10 ppb, and Hg: 6 ppb) stand out because they are persistent and non-degradable by any means of chemical and physical processes. This triad is used in batteries, petro-fuel additives, and other industrial processes, and the corresponding HMCs are among the most dangerous to human beings, especially to infants and children.[2]

Typically, pristine graphene and other forms of graphene can be functionalized using highly reactive organic intermediates such as carbocations, radicals, and nitrenes and carbenes.[3−5] All these derivatives are electron-deficient species and can accept electron donation from the graphene electronic cloud. This leads to changes in the electronic structure of graphene that can transform it from a zero-gap anomalous conductor to a non-zero-gap semiconducting material.[6−8] Furthermore, the functionalizing groups can bear organic groups such as carboxylic acid, amine, alcohols, and so forth that can serve

Received: August 16, 2021
Revised: November 13, 2021
Published: November 29, 2021

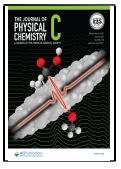

https://doi.org/10.1021/acs.jpcc.1c07247
J. Phys. Chem. C 2021, 125, 26418−26428

for further (bio)functionalization. Haloforms (i.e., chloroform, bromoform, and iodoform) and diazirines are among the most used precursors to generate carbenes upon activation with a strong base and light irradiation, respectively.[9−12] Functionalized diazirine-derived carbenes were used to modify carbon nanotubes,[13] diamond,[14] fullerene,[15] and graphene.[14,16] Similarly, aromatic azides can be cleaved to yield aromatic nitrenes, which can readily react with a carbon−carbon double bond from the graphene to yield the corresponding aziridine appendages linked to graphene.[7,8,17,18] This process was investigated theoretically and experimentally to design new nanomaterials for sensing applications.[10,19]

Recently, several authors reported the use of dihalo-(dichloro, dibromo, or diiodo)carbene to manipulate the band gap of graphene through functionalization and used it for the removal of Pb(II) from wastewater.[9,10,16,20] Moreover, Sun et al. generated diarylcarbenes from diaromatic ketones and used them to modify graphene oxide to improve its solubility in water.[21] Ismaili et al. used gold nanoparticle-tethered trifluoromethylazirine to modify reduced graphene nanosheets to form AuNP-decorated graphene.[22] This suggests the importance of investigating theoretically and experimentally the use of carbenes to modify graphene to introduce new properties, instead of dihalocarbene generated from haloforms upon basic treatment.[9,10,16]

For sensing purposes, Srivastava et al. investigated *via* density functional theory (DFT) the use of pristine graphene to sense HMCs in water such as cadmium, chromium, mercury, and lead, suggesting that the non-functionalized surface is more selective to chromium with respect to other metals.[23] Shtepliuk et al. studied the adsorption of Cd, Hg, and Pb at different oxidation degrees, namely, 0, +1, and +2 and predicted that Cd^{2+} adsorbs most strongly while Pb^{2+} adsorbs the weakest.[24] In another work, DFT and TD-DFT were used to study the adsorption of the same cations on few layers of graphene quantum dots; the highest adsorption was predicted with one layer of graphene.[25]

To gain theoretical insights in this direction, here we use DFT calculations to study the functionalization of pristine graphene with substituted carbenes and investigate their usefulness in the sensing of HMCs. We show that activated diazomethanes, as starting reagents, do not adsorb well on graphene but their carbene derivatives do and can react with graphene, via a [2 + 1]—cycloaddition, to give the corresponding substituted cyclopropanes tethered to the graphene, with reaction energies of *ca.* −1.3 to −1.8 eV. The projected density of states (PDOS) and the band structure show that the cycloaddition reaction induces a band gap opening in the graphene due to a localized graphene re-hybridization from sp^2 to sp^3. Furthermore, Löwdin partial charges and charge density differences reveal that the complexation process produces regions of charge gain or charge loss due to the hydrogen and coordination bonds. We then show that these nanomaterials interact favorably with HMCs through coordination bonds, thus allowing for their sensing. Importantly, at variance with previous studies, we employ a computational approach in which the charge of the systems is compensated via explicit counter ions rather than by a background homogeneous charge distribution. We then demonstrate that *only* after choosing a counter-ion charge compensation approach, all the four nanomaterials are predicted to interact most strongly with Pb^{2+}. This conclusion is robust with respect to inclusion of explicit solvation and can be rationalized in terms of a synergic interaction with the graphene substrate. Notably, our conclusion is *validated* by comparison with available experimental data of a larger interaction strength of Pb^{2+} with respect to Cd^{2+} for **g6×6/3b**. Grounded on this validation, we then go on to predict that, by varying the pH and following Pb^{2+} sensing and removal, the pair **g6×6/3b,c** can be employed to differentially sense Cd^{2+} and Hg^{2+} cations. In summary, we conclude that based on energetic and electronic structure analysis, such as the charge redistribution after HMC adsorption and its connection with expected response times, **g6×6/3b−d** are promising candidates to detect HMCs.

The article is organized as follow. In Section 2, we present the computational details and the method. In Section 3, we report the main results and discuss them in comparison with the relevant literature. In Section 4, we present our conclusions emphasizing the main findings and the potential application of this work.

2. COMPUTATIONAL DETAILS

The Quantum ESPRESSO (v6.5) package[26] running on XC-40 Cray Shaheen II HPC (KAUST, Saudi Arabia) was used to carry out all the ab-initio calculations. A projector-augmented wave basis set, periodic boundary conditions, and the Perdew−Burke−Ernzerhof exchange−correlation functional were used in all the calculations, and a semi-empirical Grimme's DFT-D3 (version 4) van der Waals correction was applied consistently. The energy cutoffs for the plane-wave functions and the charge density were set at 49.14 and 442.32 Ry, respectively.[19]

A graphene supercell was used, consisting of 6 × 6 unit cells (72 carbon atoms), with different modifiers physically or chemically adsorbed on it. Smaller and larger supercells were examined for comparison to validate convergence of results. During the geometry optimization (structure relaxation), the Brillouin zone was sampled using a 3 × 3 × 1 Monkhorst−Pack *k*-point grid and the orbital energies were broadened using a Gaussian smearing of 0.01 eV. All the parameters were tested to give converged results for the band structure and electronic properties. A 12 × 12 × 1 Monkhorst−Pack *k*-point grid and a tetrahedron integration method with homogeneous weights on tetrahedra were used to calculate the PDOS. For all systems, the atomic coordinates were optimized until the maximum force on ions was less than 1×10^{-3} eV/Å.

The adsorption energy of the activated diazomethanes and carbenes, ΔE_{ads}, was determined by subtracting the energies of the adsorbate ($E_{adsorbate}$) and the graphene ($E_{graphene}$) from energy of the total system ($E_{adsorbate+graphene}$) using eq 1

$$\Delta E_{ads} = E_{complex} - (E_{graphene} + E_{adsorbate}) \quad (1)$$

Similarly, in the first step, to calculate the adsorption of the metallic cations, we determined the adsorption energy by subtracting the energy of the cations (Cd^{2+}, Hg^{2+}, and Pb^{2+}) and the substrate (**g6×6/3a−d**) from the energy of the chelated complexes:

$$\Delta E_{ads} = E_{substrate/M^{2+}} - (E_{substrate} + E_{M^{2+}}) \quad (2)$$

However, as discussed in the next section, to obtain a better estimate for these charged systems, we considered a neutral supercell by adding chlorine ions as needed to neutralize the system, and the adsorption energy was calculated according to eq 3

https://doi.org/10.1021/acs.jpcc.1c07247
J. Phys. Chem. C 2021, 125, 26418−26428

$$\Delta E_{ads} = E_{substrate/MCl_2} - (E_{substrate} + E_{MCl_2}) \quad (3)$$

In the particular case of **g6×6/3c**, in which the functionalizer itself is charged or ionic, two different cases were considered starting from (i) the negatively charged carboxylate ion and M^{2+} and (ii) neutral sodium carboxylate and MCl_2. For the last scenario, the energy was calculated according to eq 4

$$\Delta E_{ads} = E_{g6\times6-3c/NaMCl_2} - (E_{substrate/Na} + E_{MCl_2}) \quad (4)$$

In fully relaxed geometries, corresponding to minimal energy of the adsorbates, substrates, and adsorbate/substrate complexes, charge density differences were calculated from fragment charge densities according to eq 5

$$\Delta\rho = \rho_{complex} - (\rho_{substrate} + \rho_{adsorbate}) \quad (5)$$

To estimate the recovery time τ, we can use an approximate analytical expression derived from the conventional transition-state theory that links recovery time to adsorption energy[27,28]

$$\tau \propto \nu^{-1} \exp(E_{ads}/k_B T) \quad (6)$$

where ν is the attempt frequency, k_B is the Boltzmann's constant, and T is the temperature. Clearly, because our adsorption energies are above 1.3 eV, they would imply too long recovery times. To restore the detection capabilities of the functionalized graphene, a laser or thermal annealing is needed to speed up desorption of the sensed species or, in some of our cases, an acidic treatment may decrease adsorption energies and allow for the release of HMCs.

All graphic, atomic, and charge density visualizations employed VESTA software (v3.5.7).[29] All geometries of the systems here investigated are depicted in Figures S1−S12 of the Supporting Information and also reported as Cartesian coordinates.

3. RESULTS AND DISCUSSION

3.1. Scope of the Study. Scheme 1 depicts the chemical structures of the activated diazomethanes and carbenes involved in the [2 + 1]—cycloaddition reaction with graphene.

Scheme 1. Schematic Representation of the Chemical Reaction Involving the C═C Bond from Graphene and the Carbene Generated from the Decomposition of the Activated Diazomethanes; (A) Diazomethane Splitting Into Carbene and N_2 and (B) Chemical Adduct between Graphene and Carbene

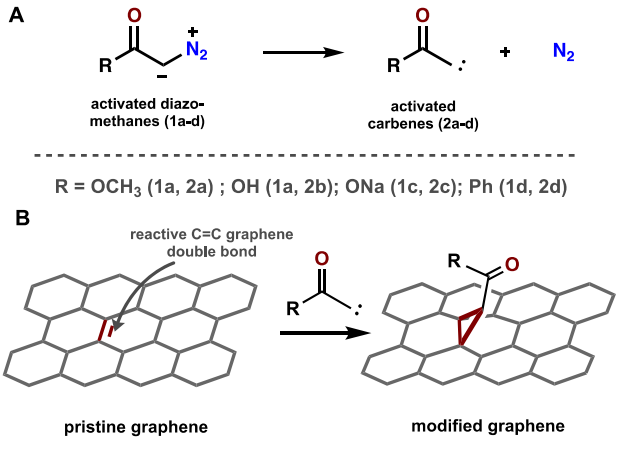

The rationale behind our choice is that the functional groups tethered to the low-valence carbene atom, after loss of a neutral N_2 molecule, will undergo a chemical reaction with a C═C bond from the graphene framework (Scheme 1). Thereafter, these functional groups can interact with the metallic cations through coordination bonds involving primarily the C═O or O−C═O groups to yield the corresponding complexes (they also can serve for further functionalization with organic molecules for interaction with proteins, but this is beyond the scope of the present work).

3.2. Physisorption of Activated Diazomethanes and Carbenes. *3.2.1. Activated Diazomethanes.* The adsorption and reaction energies were calculated according to eq 1. All the thermodynamic data and geometrical features of the physisorbed and chemisorbed compounds are summarized in Table 1, while atomistic pictures are shown in Figure 1.

The results in Table 1 show that the activated diazomethanes (**1a−d**) do not interact favorably with the pristine graphene layer neither in the vertical nor in the horizontal position with respect to the graphene surface. Indeed, the horizontal position is less favorable because some of the computed energy values are positive, indicating a repulsion between adsorbates and graphene. Compounds **1c** and **1d** give a small negative energy due to the presence of the sodium cation facing the graphene and the π-stacking of the aromatic ring on the graphene surface, respectively.[30] This conclusion is corroborated by the values of the equilibrium distances separating the involved species in a vertical configuration, which are always higher than 4.9 Å. In the case of parallel adsorption, this distance is shorter by 1.0−1.9 Å.

3.2.2. Activated Carbenes. Overall, the carbenes adsorb on the graphene surface in the vertical configuration more favorably by 0.15−0.45 eV with respect to their diazomethane precursors. It should be underlined that the adsorption energy depends on the size of the supercell. Indeed, adsorption energies for the prototypical adsorbate **2a** on supercells varying from 4 × 4 (32 atoms) to 7 × 7 (98 atoms) increase (in absolute values) from −0.02 to −0.45 eV (Table 1). The less favorable adsorption energy in the smaller supercells is due to surface stress and geometric constraints. For production calculations, we used a 6 × 6 graphene supercell, which shows a good compromise between accuracy (predicting a sizeable interaction energy) and computational effort.

The adsorption of carbenes is more favorable than that of the diazomethane precursors due to the loss of the electron-rich dinitrogen molecule and the formation of the electron-deficient activated carbenes, which interact favorably with the electronic cloud of the graphene when in a vertical position with respect to the graphene (as illustrated in Figure S13 of the Supporting Information). This is clearly illustrated by the values of the distances separating the adsorbates from the graphene, which are 3.5 to 4.0 Å, that is, ≈0.5−1.5 Å closer to graphene than the diazomethanes. In the case of adsorbate **2c**, the adsorption energy is the lowest probably due to the presence of the sodium cation in the structure and the horizontal position is favored with respect to the vertical one by −0.15 eV. This adsorbate lies 0.15 Å higher than its analogues **2a** and **2b**. For the horizontal configuration, the effect is less strong because the carbene adsorbates are closer by 0.1−0.2 Å to the graphene surface in respect to their diazomethane precursors. Finally, N_2 shows an adsorption energy of ca. −0.2 eV at all the examined positions, namely,

https://doi.org/10.1021/acs.jpcc.1c07247
J. Phys. Chem. C 2021, 125, 26418−26428

Table 1. Adsorption Energies (in eV) of the Diazomethanes and Carbenes on Graphene, and Corresponding Distances (in Å) Separating the Closest Carbon Atom from the Graphene Surface

adsorbates	1a	1b	1c	1d	2a	2b	2c	2d	N_2
ΔE_{ads} (eV)	−0.01[a]	−0.01[a]	−0.01[a]	−0.02[a]	−0.35[a]	−0.34[a]	−0.01[a]	−0.33[a]	−0.21[f]
	+0.22[b]	+0.20[b]	−0.25[b]	−0.13[b]	−0.04[b]	−0.03[b]	−0.15[b]	−0.04[b]	−0.22[g]
					−0.02[c]				−0.19[h]
					−0.21[d]				−0.21[i]
					−0.45[e]				−0.21[j]
$d_{ads\text{-}graphene}$ (Å)	4.96[a]	4.96[a]	5.02[a]	5.18[a]	3.49[a]	3.49[a]	3.66[a]	3.61[a]	4.00[f]
	3.95[b]	3.92[b]	3.09[b]	3.77[b]	3.86[b]	3.81[b]	3.56[b]	3.95[b]	3.90[g]
					3.49[c]				3.56[h]
					3.49[d]				4.01[i]
					3.49[e]				3.75[j]

[a]Vertical. [b]Horizontal positions with respect to 6 × 6. [c]Vertical position with respect to 4 × 4. [d]Vertical position with respect to 5 × 5. [e]Vertical position with respect to 7 × 7. [f]Parallel position where the two nitrogens are laying atop two carbons. [g]Parallel position where the two nitrogens are bridging. [h]Vertical in atop. [i]Vertical in bridge. [j]Vertical in hollow positions.

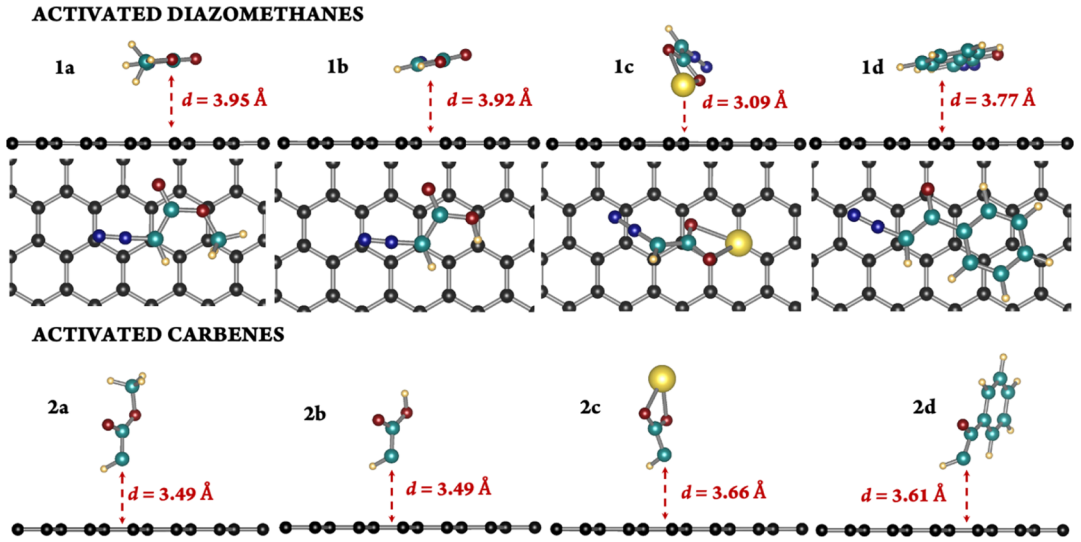

Figure 1. Selection of relaxed geometries of (top) activated diazomethanes (**1a−d**) horizontally physisorbed on the **g6×6** graphene supercell depicted from a lateral view and from a top view and (bottom) the corresponding carbenes (**2a−d**) vertically physisorbed depicted from a lateral view. Reported distances are between the closest carbon atom and the graphene surface. Color code: C: black (or cyan blue), N: dark blue, O: dark red, H: yellow, and Na: light yellow. The color of adsorbate carbons is set to cyan-blue for clarity.

two parallel, atop, bridge, and hollow positions, which is consistent with previous findings.[19]

3.3. Chemical Reaction of the Activated Carbenes with Graphene. Table 2 displays the values of [2 + 1]—cycloaddition reaction energy of the four functionalizing groups with graphene. Most of the energies are strongly negative (ca. −1.3 to −1.8 eV), denoting a much more favorable chemical process than physical adsorption. These values are in good agreement with previous literature values.[6,12,19] Again, in the case of adsorbate **2c**, the reaction energy is the weakest probably due to the presence of the sodium cation in the adsorbate.

Also in this case the reaction energy is dependent on the size of the supercell but to a relatively lesser degree, implying that our production systems are sufficiently large to give accurate results. Indeed, the reaction energy value increases (in absolute values) from −1.43 to −1.56 eV, when the supercell size increases from 32 carbon atoms (i.e., 4 × 4 supercell) to 98 carbon atoms (i.e., 7 × 7 supercell), again due to a lesser surface stress and geometric constraints caused by the cycloaddition reaction. Incidentally, this implies that it becomes progressively more difficult to increase the density of cyclopropane appendages on the graphene surface due to the disruption of its electronic cloud and geometric deformation.[6]

Once the carbenes react with the graphene surface, two carbons from the graphene undergo a change in hybridization from sp^2 to sp^3. The geometrical features of the as-formed cyclopropanes support this conclusion because the C−C bond lengths (d_1 to d_3) range from 1.52 to 1.57 Å, which are typical of sp^3−sp^3 carbon−carbon bonds (Figure 2). These distances are close to those found by Zan in a study of a series of R_2C (R = H, H_3C, Ph, NO_2, CN, and Cl) on graphene sheets.[12] Furthermore, the graphene structure changes locally to exhibit a protuberance of *ca.* 0.6 to 0.7 Å above the graphene mean surface, which progressively disappears toward the borders of the unit cell.[6] The values of the internal cyclopropane α angle and the β angle involving the sp^3 graphene carbon and its adjacent neighbors are approximately 60 and 117°, which are typical of small constrained three-membered cycles and sp^3-hybridized carbons.

https://doi.org/10.1021/acs.jpcc.1c07247
J. Phys. Chem. C 2021, 125, 26418−26428

Table 2. [2 + 1]—Cycloaddition Reaction Energies and Geometrical Features of the Cyclopropane-Modified Graphene Nanomaterials (See Figure 2 for Their Definition)

adsorbates	energy (eV)	geometrical features
3a	−1.49[a]	d_1: 1.56
	−1.56[b]	d_2: 1.52
	−1.46[c]	d_3: 1.55
	−1.43[d]	d_4: 1.22
		d_5: 1.37
		h: 0.72
		α: 60.88
		β: 118.16
3b	−1.77[a]	d_1:1.55
		d_2: 1.55
		d_3: 1.54
		d_4: 1.22
		d_5: 1.36
		h: 0.71
		α: 60.20
		β: 117.51
3c	−1.35[a]	d_1:1.57
		d_2: 1.54
		d_3: 1.54
		d_4: 1.26
		d_5: 1.26
		h: 0.62
		α: 61.50
		β: 117.65
3d	−1.41[a]	d_1: 1.54
		d_2: 1.57
		d_3: 1.54
		d_4: 1.23
		d_5: n.a.
		h: 0.66
		α: 59.41
		β: 117.50

[a]6 × 6. [b]4 × 4. [c]5 × 5. [d]7 × 7 graphene supercells; d_1: C1−C2 length (Å), d_2: C2−C3 length (Å), d_3: C1−C3 length (Å), d_4: C═O length (Å), d_5: C−O length (Å), h: elevation of C1 and C3 in respect to the mean level of the graphene (Å), α: angle C1−C2−C3 (deg), and β: C−C1−C (deg); n.a.: not applicable.

Change from methyl ester to carboxylic acid to the sodium carboxylate group can be monitored from the length of C−O bonds (d_4 and d_5 in Table 2), which varies from disproportionated lengths (1.22 and 1.37 Å) in the case of methyl ester to symmetrical bonds of length 1.26 Å in the case of the sodium carboxylate group.

Although DFT calculations correspond to modeling at 0 K, the cycloadducts should be stable at ambient temperature. Indeed, Sakar et al.[31] and others[32] showed the [4 + 2] cycloaddition reaction of diene compounds with graphene occurs at temperatures ranging from 50 to 130 °C depending on the diene. The reverse reaction only occurs at temperature above 160 °C and restores the initial graphene.

3.4. Electronic Structure Analysis. To gain further insight into the modification to the electronic properties of the system following functionalization and HMC adsorption, we report in Figure 3 the electronic bands (panels A and B) and PDOS (panel C) plots for pristine graphene **g6×6** (panels A−C), one example of functionalized graphene, **g6×6/3d** (panel A), and **g6×6/3d** interacting with Pb^{2+} in the case of the explicit counter-ion approach, the **g6×6/3d-PbCl$_2$** system; see Section 3.5.2 below (panels B and C) and a depiction of this last system (panel D).

In Figure 3C, the PDOS of **g6×6/3d-PbCl$_2$** is projected on three representative carbon atoms, indicated as atom A, B, and C in panel **3**(D) in order of increasing geometric distance from the functionalizing group. From the comparison of the band structure of pristine graphene (red curve in panels A and B of Figure 3) and the functionalized **g6×6/3d** system (green curve in panel A of Figure 3), one can first see the expected partial band gap opening induced by the functionalization, as discussed in previous work.[12,19] The proposed sensing mechanism in these materials is related to the change in electronic transmission upon adsorption. An ideal sensing material should have a high carrier mobility, a narrow band gap, and a high response of electronic transmission to adsorption of sensed species, for example, a shift in the position of the minimum of transmission after adsorption. In this perspective, the changes after cation adsorption in the band structure of the functionalized system (panel B vs panel A in Figure 3) and PDOS (panel C in Figure 3) after Pb^{2+} adsorption are interesting; these significant changes should translate into a corresponding, experimentally detectable change in transmission and, therefore, be amenable for sensing purposes.

3.5. Detection of HMCs. *3.5.1. Detection of Cations Using Charged Supercells.* Because the different appendages of graphene bear electron-rich oxygen functional groups, we examined their potential use as chelating agents for HMCs such as Pb^{2+}, Cd^{2+} and Hg^{2+}. In the first step, we studied the interaction between the functionalized graphene (**g6×6/3a−d**) and charged metallic cations along the lines of a similar work by Srivastava[23] and Shtepliuk.[24] The interaction energy was calculated using eq 2, and the thermodynamic data are gathered in Table 3.

From these results, we can see that all the compounds interact favorably with the cations with large interaction energies, in all cases more negative than −9.8 eV. These energies are consistent with those reported by Shtepliuk et al.,[24] who find −7.05, −14.56, and −11.63 eV, respectively, for Pb^{2+}, Hg^{2+}, and Cd^{2+} laying at equilibrium distances ranging from 2.22 to 3.39 Å. In our case, the equilibrium distances are similar and range from 2.23 to 4.36 Å. A selection of the optimized geometries is gathered in Figure 4. The results would predict that mercury and cadmium interact much more strongly than lead cations with energies almost twice than those obtained for Pb^{2+} except for **g6×6/3b**.

Furthermore, the Cd^{2+}···O═C bond length shortens from 4.36 to 2.32 Å when the chelating group changes from an ester (−CO_2Me) to a carboxylic acid (−CO_2H) to a carboxylate (−CO_2Na) having higher coordination power and available pair of electrons. Mercury is the least attracted to oxygen because equilibrium distances are longer than 3.0 Å (except for **g6×6/3c**), which can be explained by a higher affinity of mercury cations to softer ligands containing sulfur and phosphorus atoms.[33] In the case of Pb^{2+} and Cd^{2+} interacting with **g6×6/3c**, the equilibrium distances (Cd···O: 2.31 Å, Hg···O: 2.28 Å, and Pb···O: 2.45 Å) are approximately equal to the sum of ionic radii of the atoms, denoting that the carboxylate anion interacts strongly with the three metallic cations to form bichelated complexes involving the two

https://doi.org/10.1021/acs.jpcc.1c07247
J. Phys. Chem. C 2021, 125, 26418−26428

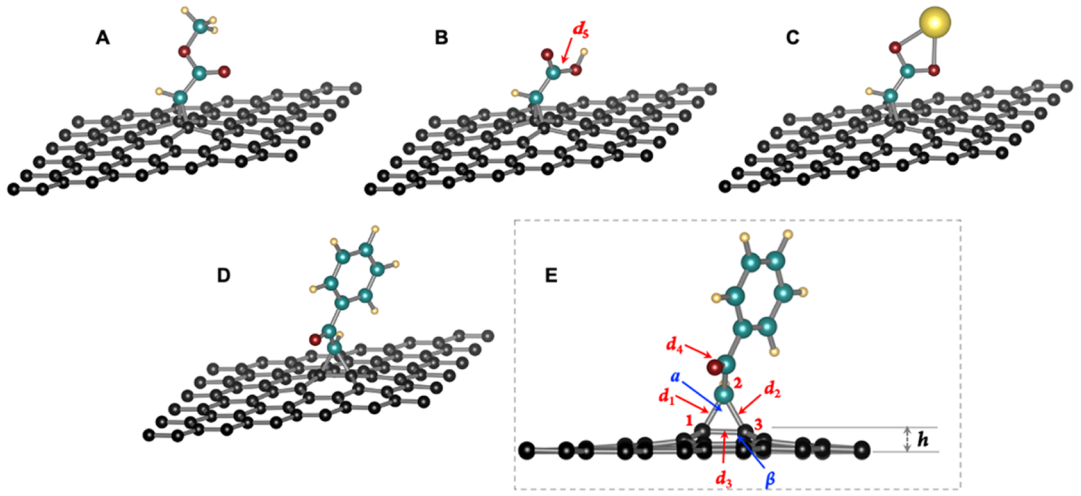

Figure 2. (A–D) Geometries of the optimized cyclopropane appendages to the graphene supercell (**g6×6/3a–d**). Boxed structure (E) illustrates the geometrical features that are gathered in Table 2. Angles are indicated by blue arrows and bond lengths by red arrows. Atom labels (1, 2, and 3) indicate the atoms involved in the cycloaddition reaction. The color code of the atoms is the same as in Figure 1.

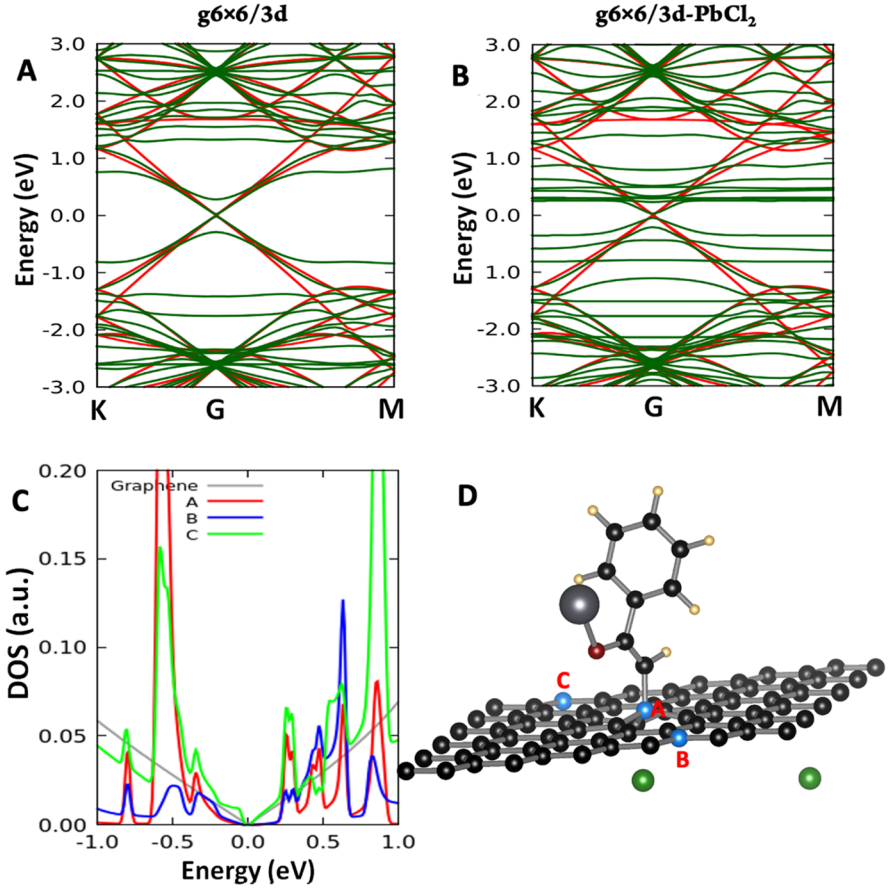

Figure 3. (A,B) Electronic band structure plots and (C) PDOS for pristine graphene **g6×6**, functionalized graphene **g6×6/3d** and (D) pictorial atomistic depiction of the interaction complex of **g6×6/3d** with Pb^{2+}, the **g6×6/3d-PbCl$_2$** system. In panels A and B, the graphene bands are in red and those of the functionalized systems are in green. In panel C, the zero of energy is set to the *K* point of graphene or functionalized graphene; the carbon atoms on which the PDOS are projected are indicated in the inset and correspond to the atomistic picture of panel D. Color coding in panel D: hydrogen = light orange, carbon = black, lead = large gray sphere; oxygen = red, and chlorine (added anions) = green. All energies are in eV.

oxygens of the carboxylate group.[34] In all cases, the cations form slightly asymmetrical complexes with the ligands.

3.5.2. Detection of Cations Using Neutral Supercells. Experimental evidence shows that Pb^{2+} has more affinity to carboxylic acid than to softer Cd^{2+} and Hg^{2+}cations. Bala et al. studied experimentally the interaction between metal ions (Ca^{2+}, Co^{2+}, Pb^{2+}, and Cd^{2+}) and the carboxylic acid and found that the strength of binding of the different cations varies as

https://doi.org/10.1021/acs.jpcc.1c07247
J. Phys. Chem. C 2021, 125, 26418–26428

Table 3. Adsorption Energies of the HMCs, Atoms Involved in the Coordination Bonds, and the Lengths of the Coordination Bonds between the Oxygen and the Metal Ions

substrates	cations	energy (eV)	involved atoms	d_O−M^{2+} (Å)
G6×6/3a	Cd^{2+}	−14.62	C═O···Cd^{2+}	4.36
	Hg^{2+}	−17.57	C═O···Hg^{2+}	4.35
	Pb^{2+}	−09.83	C═O···Pb^{2+}	2.23
G6×6/3b	Cd^{2+}	−14.30	C═O···Cd^{2+}	4.01
	Hg^{2+}	−29.27	C═O···Hg^{2+}	3.02
	Pb^{2+}	−25.46	C═O···Pb^{2+}	2.27
G6×6/3c	Cd^{2+}	−16.65	CO_2^-···Cd^{2+}	2.32/2.42
	Hg^{2+}	−19.04	CO_2^-···Hg^{2+}	2.48/2.86
	Pb^{2+}	−13.90	CO_2^-···Pb^{2+}	2.27/2.31
G6×6/3d	Cd^{2+}	−14.67	C═O···Cd^{2+}	3.26
	Hg^{2+}	−17.76	C═O···Hg^{2+}	3.54
	Pb^{2+}	−11.99	C═O···Pb^{2+}	2.19

Ca^{2+} > Co^{2+} > Pb^{2+} > Cd^{2+}.[35] This contradicts the results in Table 3 that cadmium and mercury interact more strongly than lead with the different oxygen-bearing nanomaterials (Cd^{2+} > Pb^{2+} and Hg^{2+} > Pb^{2+}). The reason of this failure of the theoretical approach can be traced back to the use of charged supercells (i.e., in which the physical system is charged and a fictitious homogeneous charged background is introduced to avoid electrostatic divergence), and the resulting issue of how to deal with the electrostatic interactions in 3D periodic codes, which may lead to erroneous results. To correct for these errors and arrive at an accurate description of the physics of cation absorption on the functionalized systems, we adopted an alternative approach in which the positive charges of the cations are compensated with two chlorine atoms being positioned at remote locations with respect to the cations on the substrates **g6×6/3a**, **g6×6/3b**, and **g6×6/3d** (as anticipated, for convenience of the reader in the Supporting Information, we report atomistic pictures and Cartesian coordinates of all the systems here investigated). Equations 3 and 4 were used to calculate the interaction energies, which are gathered in Table 4. These results show that, in all cases, the interaction with Pb^{2+} yields a binding stronger by 40−76% for **g6×6/3a**, **g6×6/3b**, and **g6×6/3d** with respect to the two other cations and in particular that this is true for the **g6×6/3b** case, which corresponds to the experiment of ref 35 (note that for **g6×6/3c**, the interactions with Cd^{2+} are weaker than those with Pb^{2+} by only ≈5%). Interestingly, in the **g6×6/3c** case, the order of interaction strength between Cd^{2+} and Hg^{2+} cations is reversed, with the softer Cd^{2+} species binding stronger than the harder Hg^{2+}. This is important because it suggests that by varying the pH, one can use **g6×6/3b** and **g6×6/3c** nanomaterials to achieve *selective (differential) sensing* of Cd^{2+} with respect to Hg^{2+} cations.

Additionally, to probe the solvent effect, we added one or two water molecules to the complex. The results show that the presence of the water molecules exerts an important effect because the overall interaction energy with cations dropped by 0.16−0.89 eV, depending on the number of water molecules surrounding the complex (entries 4−6 in Table 4). The C═O···M^{2+} distance remains almost the same, except for the mercury(II) complex, where the ion moves away by 0.2 Å with respect to their initial equilibrium distance. The new H_2O···M^{2+} distances are approximately equal to their respective C═O···M^{2+} distance. Also, the different complexes **g6×6/3b**-M^{2+} are found to be 2.17−2.96 eV more stable in water than in a vacuum using the self-consistent continuum solvation (SCCS) model provided by the Environ plugin.[26] Unfortunately, the interaction energy cannot be estimated using SCCS because the overlapping of the continuum fields between the substrate and the metallic cations produces erroneous results.

Note that the results in Table 4 show that the interaction energy ranges from −1.18 to −2.75 eV (−113.9 and −265.3 kJ/mol), which is 1 order of magnitude less that that given in Table 3 in the charged unit cell approach. An important point to emphasize is that the values of interaction energies in the charged unit cell approach are indeed extremely high (between −9.83 and −29.27 eV or between −948.5 and −2824.1 kJ/mol) and are not physically acceptable because the bond dissociation energies of most Pb^{2+} compounds do not exceed

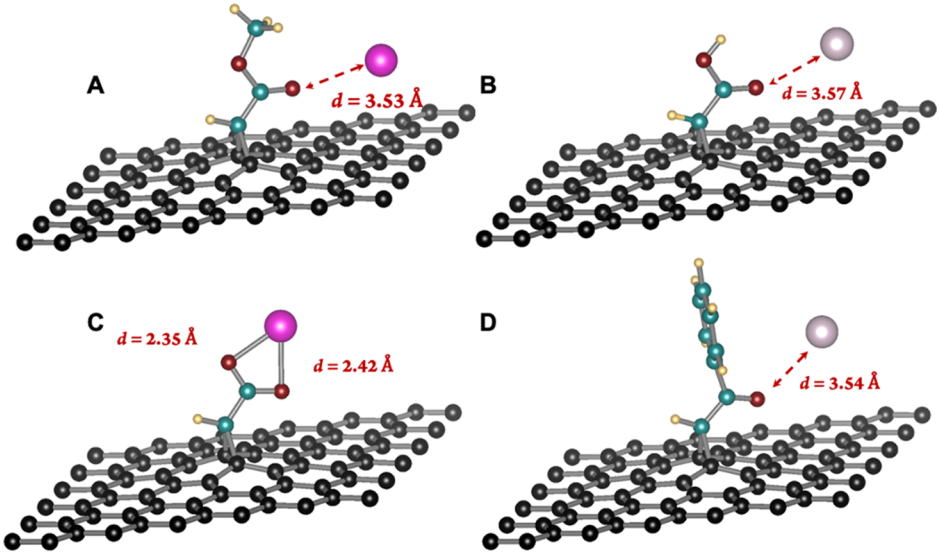

Figure 4. Selection of the optimized geometries of **g6×6/3a−d** interacting with metallic cations (A) **g6×6/3a-Cd^{2+}**, (B) **g6×6/3b-Hg^{2+}**, (C) **g6×6/3c-Cd^{2+}**, and (D) **g6×6/3d-Hg^{2+}**. The coordination bond lengths are indicated near the interacting atoms. The color code of the atoms is given in Figure 1.

https://doi.org/10.1021/acs.jpcc.1c07247
J. Phys. Chem. C 2021, 125, 26418−26428

Table 4. Adsorption Energies of the HMCs, Atoms Involved in the Coordination Bonds, and Distances Separating Them from the Graphene Surface

Substrates	Cations	Energy (eV)	Involved atoms	$d_{O\text{-}M^{2+}}$ / $d_{H2O\text{-}M^{2+}}$ (Å)
G6×6/3a	Cd^{2+}	−1.62	C=O···Cd^{2+}	3.53
	Hg^{2+}	−1.90	C=O···Hg^{2+}	3.64
	Pb^{2+}	−2.66	C=O···Pb^{2+}	2.38
G6×6/3b	Cd^{2+}	−1.62[a]/−1.38[b]/−1.28[c]	C=O···Cd^{2+}/HO···Cd^{2+}	3.28[d](3.37[e])/3.17[f]
	Hg^{2+}	−1.90[a]/−1.76[b]/−1.74[c]	C=O···Hg^{2+}/HO···Hg^{2+}	3.57[d](3.76[e])/3.82[f]
	Pb^{2+}	−2.66[a]/−1.99[b]/−1.77[c]	C=O···Pb^{2+}/HO···Pb^{2+}	2.39 [d](2.40[e])/2.68[f]
G6×6/3c	Cd^{2+}	−1.73	CO_2^-···Cd^{2+}	2.35/2.42
	Hg^{2+}	−1.18	CO_2^-···Hg^{2+}	2.96/3.30
	Pb^{2+}	−1.82	CO_2^-···Pb^{2+}	2.28/2.30
G6×6/3d	Cd^{2+}	−1.56	C=O···Cd^{2+}	4.29
	Hg^{2+}	−1.83	C=O···Hg^{2+}	3.54
	Pb^{2+}	−2.75	C=O···Pb^{2+}	2.18

[a]Bare complex in a vacuum. [b]Monohydrated complex in a vacuum. [c]Dihydrated complex in a vacuum. [d]C=O···M^{2+} distance for the bare complex in a vacuum. [e]C=O···M^{2+} distance for the dihydrated complex in a vacuum. [f]HO···M^{2+} distance for the dihydrated complex in a vacuum.

−380 kJ/mol (−3.94 eV).[36] In contrast, the interaction energies in the explicit counter-ion approach are much smaller and physically reasonable. Nevertheless, it is also important to stress that the interaction strength even in the weakest case (1.18 eV) is still sufficient to absorb concentrations down to 10^{-20} M and is thus appropriate to detect ppb levels as required by the present legislation (USEPA Clean Water Act).[37]

3.6. Differences in Electronic Charge Densities. To further analyze the interaction between the **g6×6/3a−d** complexes and the metal cations, we used eq 5 to estimate the difference in charge densities and unveil charge transfer between the species. The corresponding results are depicted in Figure 5. From this figure, we see that due to the high charge of the metallic cations, there is a strong charge transfer from the appendages to the cations (blue areas) that even propagate to the graphene supercell. The oxygens involved in the binding are the atoms that donate most to the cations (Figure 5). In the case of the **g6×6/3d-Pb^{2+}** complex, the strong interaction induced a larger charge transfer from the oxygen and from the carbons and the hydrogens of the aromatic ring.

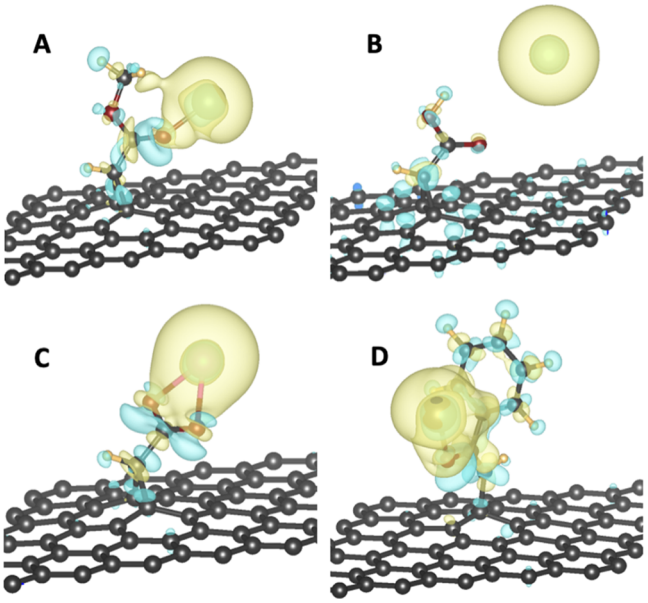

Figure 5. Plots of differences in electron density showing regions of charge depletion (blue color) or charge gain (yellow color) around the metallic cations. Isovalues of the charge density differences were set at 5 × 10^{-3} e/bohr^3. (A) **g6×6/3a-Pb^{2+}**, (B) **g6×6/3b-Hg^{2+}**, (C) **g6×6/3c-Cd^{2+}**, and (D) **g6×6/3d-Pb^{2+}**.

3.7. Adsorption of Lead(II) Cations. Here, we focus our attention on the adsorption of Pb^{2+}, which is the most favorable cation energetically and also the most complex/interesting from the chemical point of view, as we show below.

3.7.1. Geometrical Features. From the study of the charge density differences (Figure 5), it results that Pb^{2+} interacts strongly with the aromatic ring of the functionalizer in the **g6×6/3d** case. Similarly, the results show that Pb^{2+} not only forms strong bonds with C=O groups from **g6×6/3a** and **g6×6/3b** but also interacts significantly with the graphene substrate because the Pb···C_{gr} distance is 2.48 and 2.29 Å, respectively (Figure 6), although these distances are 17−26% longer than the sum of ionic radii of carbon and lead (1.96 Å). The hard Pb^{2+} is not only attracted to the oxygens but also to the graphene electron cloud and its electron-donating properties.

Moreover, by analyzing these structures in more detail, we find that, unexpectedly, in the case of **g6×6/3d**, geometry relaxation leads to the opening of the cyclopropane ring to give a conjugated enolic form, where the oxygen is ionically linked to Pb^{2+}. Figure 6D depicts the initial position of the aromatic ring (gray atoms) and the final position (cyan atoms). Indeed, the C_1-C_2 bond remains almost of the same length (1.57 Å), whereas the C_2-C_3 bond shortens by 0.13 Å to become a double bond while simultaneously the C_3-O bond increases by 0.12 Å to form a single bond. In this case, the Pb−O bond is shorter than the sum of ionic radii of Pb^{2+} and oxygen, denoting a strong interaction.[34] Furthermore, the relaxed Pb^{2+} position is at a short distance from the nucleus of the aromatic ring (3.25 Å) and a long distance from graphene (4.91 Å).

3.7.2. Electron Density and Lowdin Charges. To gain further insight into the adsorption of Pb^{2+}, we also examined the charge density variations around the involved atoms. Displayed in Figure 7A,B, isocontour plots indicate regions of charge loss (colored in blue) and regions of charge gain (colored in yellow). Particularly, for **g6×6/3a-Pb^{2+}**, we notice a huge charge withdrawal from the six graphene atoms lying vertically under Pb^{2+} and also from the oxygen and the chlorine atoms toward the lead(II) cation. Similarly, in the **g6×6/3d-Pb^{2+}** complex, the charge loss occurs from the aromatic ring of the functionalizer **3d**, which in turn withdraws electronic density from the graphene.[38] The chlorine under the graphene

https://doi.org/10.1021/acs.jpcc.1c07247
J. Phys. Chem. C 2021, 125, 26418−26428

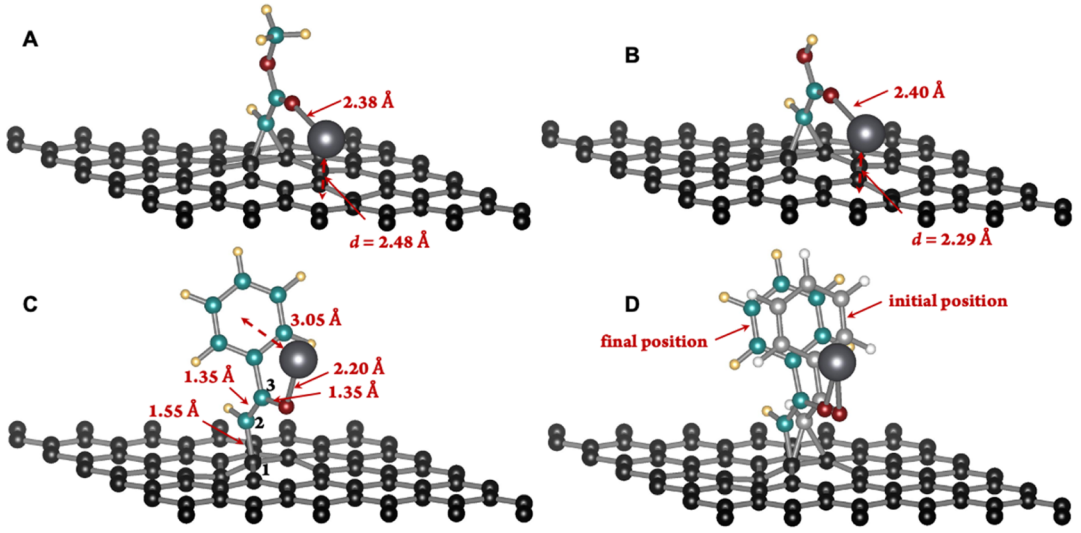

Figure 6. Selection of optimized geometries of (A) **g6×6/3a**, (B) **g6×6/3b**, and (C) **g6×6/3d** interacting with Pb^{2+}. The coordination bond lengths are also indicated. (D) In the case of **g6×6/3d**, display of the initial and final positions of the organic functionalizer before and after isomerization induced by interaction with Pb^{2+} (see text for details). The color code of the atoms is the same as in Figure 1.

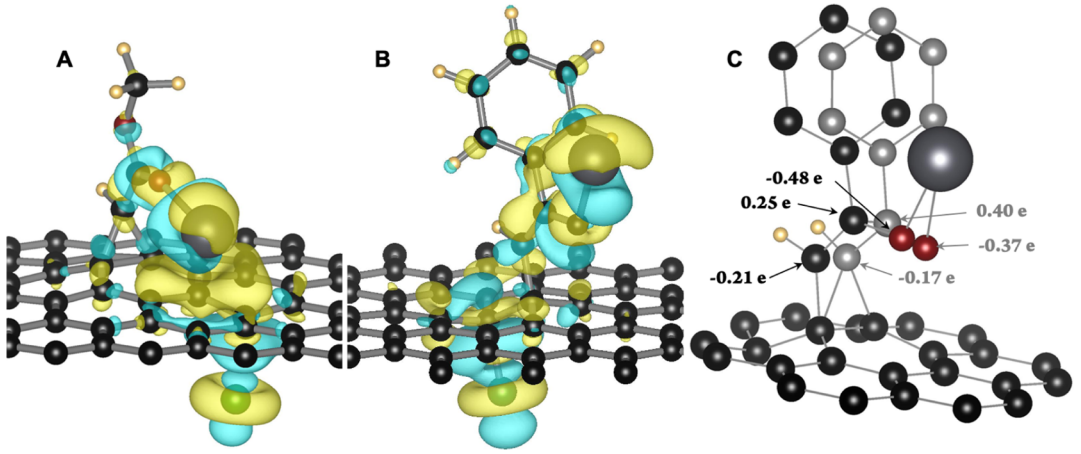

Figure 7. Isovalue plot of charge density differences showing regions of charge loss (blue) and regions of charge gain (yellow) for the atoms involved in the interaction in (A) **g6×6/3a-Pb^{2+}** and (B) **g6×6/3d-Pb^{2+}**. Isovalues of the charge density differences were set at 2.5×10^{-3} e/bohr^3. (C) **g6×6/3d-Pb^{2+}** system before and after isomerization. The Löwdin partial charges are indicated in gray (before) and black (after). Many atoms were omitted for clarity.

layer come closer to the graphene to compensate for the charge density loss (1.95 Å).

We further computed Löwdin partial charges, and we report in Figure 7C the corresponding charge changes after the interaction with Pb^{2+}. The charge gain on the cyclopropane carbon increased by $-0.04e$, while the charge loss on the carbonyl carbon drops from $+0.40e$ to $+0.25e$ by gaining electron density from the graphene electronic cloud. Finally, the change of oxygen from the carbonyl form (C═O) to the enolate form ($C-O^-$) comes with a density gain of $-0.11e$ comes with a density gain to Pb^{2+}, which gains $-0.12e$ (net charge varies from +1.41 to +1.29).

3.7.3. Response Time. In addition to recovery time, another important quantity for assessing the possible use of the systems here investigated in real sensing devices is the response time. There is some ambiguity on this topic in the literature, and the definition and measurement under precisely defined conditions (primarily, concentration) of recovery times are not easily found. However, the usual consensus is that the response time correlates with charge transfer (see, e.g., ref 39). Because in Figure 7C we find Lowdin charge differences of $0.12-0.15e$, we can estimate that this amount of charge transfer should give rise to quick response times, and thus, HMC adsorption should be amenable to fast sensing.

4. CONCLUSIONS

Introducing functional groups with tailored properties into graphene can be of great interest in current physico-chemical research on sensing applications for the detection of HMCs and the assessment of contaminants that are dangerous for public safety. In the present work, we show that pristine graphene can be modified with four functionalized carbenes, RCOCH, with R = $-OCH_3$ (**2a**), −OH (**2b**), −ONa (**2c**), and −Ph (**2d**), generated from the corresponding activated diazomethanes, to yield the corresponding cyclopropane-modified graphene derivatives, representing an original path to covalently modify graphene materials. We find that the reactions are thermodynamically favored and occur with

https://doi.org/10.1021/acs.jpcc.1c07247
J. Phys. Chem. C 2021, 125, 26418−26428

reaction energies ranging from −1.35 to −1.8 eV. A combined band structure and PDOS analyses show the opening of a local energy band gap, yielding a semiconducting state of graphene, which may make it suitable for sensing applications, although dependent upon the density of modifiers as a key parameter. Our modeling suggests that **g6×6/3b−d** can be used to sense HMCs, such as Cd^{2+}, Hg^{2+}, and Pb^{2+} investigated in the present work as the most common and harmful HMCs. Indeed, the interaction of these HMCs via coordination bonds with the functional groups anchored on graphene induces appreciable charge density differences in the system, which should be experimentally detectable. Moreover, after and *only* after properly introducing explicit counter-ions in our modeling, we predict that Pb^{2+} interacts more strongly than Cd^{2+} (and Hg^{2+}) with the **g6×6/3b−d** complexes, which is in perfect agreement with experimental data. Grounded on this validation, we go on to predict that, by varying the pH and following Pb^{2+} sensing and removal, the pair **g6×6/3b,c** can be employed to differentially sense Cd^{2+} and Hg^{2+} cations.

The proof-of-concept approach here explored can be extended to other host−receptor pairs chemisorbed on graphene and represents a promising path to prepare a whole series of sensing devices based on graphene (and possibly other 2D materials).

■ ASSOCIATED CONTENT

Supporting Information

The Supporting Information is available free of charge at https://pubs.acs.org/doi/10.1021/acs.jpcc.1c07247.

Atomistic pictures and Cartesian coordinates of the structural models discussed in the main text (PDF)

■ AUTHOR INFORMATION

Corresponding Authors

Alessandro Fortunelli − *Consiglio Nazionale delle Ricerche, CNR-ICCOM, Pisa 56124, Italy;* orcid.org/0000-0001-5337-4450; Email: alessandro.fortunelli@cnr.it

Adnene Dhouib − *Department of Chemistry, College of Science, Imam Abdulrahman Bin Faisal University, Dammam 31113, Saudi Arabia*; Email: amdhouib@iau.edu.sa

Noureddine Raouafi − *Laboratory of Analytical Chemistry and Electrochemistry (LR99ES15), Chemistry Department Faculty of Science of Tunis, University of Tunis El Manar, Tunis El Manar 2092, Tunisia;* orcid.org/0000-0001-8938-8221; Email: noureddine.raouafi@fst.utm.tn

Authors

Sabrine Baachaoui − *Laboratory of Analytical Chemistry and Electrochemistry (LR99ES15), Chemistry Department Faculty of Science of Tunis, University of Tunis El Manar, Tunis El Manar 2092, Tunisia*

Sarah Aldulaijan − *Department of Chemistry, College of Science, Imam Abdulrahman Bin Faisal University, Dammam 31113, Saudi Arabia*

Luca Sementa − *Consiglio Nazionale delle Ricerche, CNR-ICCOM & IPCF, Pisa 56124, Italy*

Complete contact information is available at: https://pubs.acs.org/10.1021/acs.jpcc.1c07247

Author Contributions

S.B.: investigation, data curation, and writing—original draft; S.A.: Investigation and data curation; L.S.: investigation, validation, and supervision; A.F.: methodology and writing—review and editing; A.D.: investigation, supervision, and review and editing; N.R.: methodology, supervision, validation, and writing—review and editing.

Notes

The authors declare no competing financial interest.

■ ACKNOWLEDGMENTS

For computer time, this research (ref. k1396) used the resources of the Supercomputing Laboratory at King Abdullah University of Science & Technology (KAUST) in Thuwal, Saudi Arabia.

■ REFERENCES

(1) World Health Organization's WHO. *Guidelines for Drinking-Water Quality*, 4th ed; World Health Organization: Geneva, 2011.

(2) Ferguson, A.; Penney, R.; Solo-Gabriele, H. A Review of the Field on Children's Exposure to Environmental Contaminants: A Risk Assessment Approach. *Int. J. Environ. Res. Publ. Health* **2017**, *14*, 265.

(3) Han, J.; Gao, C. Functionalization of Carbon Nanotubes and Other Nanocarbons by Azide Chemistry. *Nano-Micro Lett.* **2010**, *2*, 213−226.

(4) Park, J.; Yan, M. Covalent Functionalization of Graphene with Reactive Intermediates. *Acc. Chem. Res.* **2013**, *46*, 181−189.

(5) Chua, C. K.; Pumera, M. Covalent Chemistry on Graphene. *Chem. Soc. Rev.* **2013**, *42*, 3222−3233.

(6) Hildebrand, M.; Abualnaja, F.; Makwana, Z.; Harrison, N. M. Strain Engineering of Adsorbate Self-Assembly on Graphene for Band Gap Tuning. *J. Phys. Chem. C* **2019**, *123*, 4475−4482.

(7) Choi, J.; Kim, K.-j.; Kim, B.; Lee, H.; Kim, S. Covalent Functionalization of Epitaxial Graphene by Azidotrimethylsilane. *J. Phys. Chem. C* **2009**, *113*, 9433−9435.

(8) Suggs, K.; Reuven, D.; Wang, X.-Q. Electronic Properties of Cycloaddition-Functionalized Graphene. *J. Phys. Chem. C* **2011**, *115*, 3313−3317.

(9) Sainsbury, T.; Passarelli, M.; Naftaly, M.; Gnaniah, S.; Spencer, S. J.; Pollard, A. J. Covalent Carbene Functionalization of Graphene: Toward Chemical Band-Gap Manipulation. *ACS Appl. Mater. Interfaces* **2016**, *8*, 4870−4877.

(10) Li, H.-Y.; Yue, B.-Y.; Yu, J.-G.; Wu, X.-W.; Zhou, W.-X.; Zhou, N.; Teng, J.; Zhong, M. Diiodocarbene Modified Graphene: Preparation, Characterization and Its Application as a Novel Adsorbent for Aqueous Removal of Pb(Ii). *Nanosci. Nanotechnol. Lett.* **2016**, *8*, 387−392.

(11) Yan, W.; Xu, Y.; Chen, Y. Facile and Effective Functionalization of Graphene Oxide by Boron-Oxygen Covalent or Bingel Cyclopropanation Reaction. *J. Nanosci. Nanotechnol.* **2015**, *15*, 2020−2026.

(12) Zan, W. Chemical Functionalization of Graphene by Carbene Cycloaddition: A Density Functional Theory Study. *Appl. Surf. Sci.* **2014**, *311*, 377−383.

(13) Lawrence, E. J.; Wildgoose, G. G.; Aldous, L.; Wu, Y. A.; Warner, J. H.; Compton, R. G.; McNaughter, P. D. 3-Aryl-3-(Trifluoromethyl)Diazirines as Versatile Photoactivated "Linker" Molecules for the Improved Covalent Modification of Graphitic and Carbon Nanotube Surfaces. *Chem. Mater.* **2011**, *23*, 3740−3751.

(14) Hesari, M.; Workentin, M. S. Covalent Modification of Graphene and Micro-Diamond with Redox Active Substrates Via Photogenerated Carbenes. *Carbon* **2015**, *85*, 159−167.

(15) Yamada, M.; Someya, C. I.; Nakahodo, T.; Maeda, Y.; Tsuchiya, T.; Akasaka, T. Synthesis of Endohedral Metallofullerene Glycoconjugates by Carbene Addition. *Molecules* **2011**, *16*, 9495−9504.

(16) Chua, C. K.; Ambrosi, A.; Pumera, M. Introducing Dichlorocarbene in Graphene. *Chem. Commun.* **2012**, *48*, 5376−5378.

(17) Yang, X.; Chen, F.; Kim, M. A.; Liu, H.; Wolf, L. M.; Yan, M. On the Reactivity Enhancement of Graphene by Metallic Substrates Towards Aryl Nitrene Cycloadditions. *Chemistry* **2021**, *27*, 7887−7896.
(18) Abuelela, A. M.; Farag, R. S.; Mohamed, T. A.; Prezhdo, O. V. Ab Initio Study of the Vibrational Signatures for the Covalent Functionalization of Graphene. *J. Phys. Chem. C* **2013**, *117*, 19489−19498.
(19) Baachaoui, S.; Aldulaijan, S.; Raouafi, F.; Besbes, R.; Sementa, L.; Fortunelli, A.; Raouafi, N.; Dhouib, A. Pristine Graphene Covalent Functionalization with Aromatic Aziridines and Their Application in the Sensing of Volatile Amines - an Ab Initio Investigation. *RSC Adv.* **2021**, *11*, 7070−7077.
(20) Teng, J.; et al. Dibromocarbene Modified Graphene: Preparation, Characterization and Its Application in Removal of Pb(Ii) from Aqueous Solutions. *Nanosci. Nanotechnol. Lett.* **2016**, *8*, 226−231.
(21) Sun, Z.; Guo, D.; Wang, S.; Wang, C.; Yu, Y.; Ma, D.; Zheng, R.; Yan, P. Efficient Covalent Modification of Graphene by Diazo Chemistry. *RSC Adv.* **2016**, *6*, 65422−65425.
(22) Ismaili, H.; Geng, D.; Sun, A. X.; Kantzas, T. T.; Workentin, M. S. Light-Activated Covalent Formation of Gold Nanoparticle Graphene and Gold Nanoparticle-Glass Composites. *Langmuir* **2011**, *27*, 13261−13268.
(23) Srivastava, M.; Srivastava, A.; Pandey, S. K. Suitability of Graphene Monolayer as Sensor for Carcinogenic Heavy Metals in Water: A Dft Investigation. *Appl. Surf. Sci.* **2020**, *517*, 146021.
(24) Shtepliuk, I.; Caffrey, N. M.; Iakimov, T.; Khranovskyy, V.; Abrikosov, I. A.; Yakimova, R. On the Interaction of Toxic Heavy Metals (Cd, Hg, Pb) with Graphene Quantum Dots and Infinite Graphene. *Sci. Rep.* **2017**, *7*, 3934.
(25) Shtepliuk, I.; Yakimova, R. Interband Absorption in Few-Layer Graphene Quantum Dots: Effect of Heavy Metals. *Materials* **2018**, *11*, 1217.
(26) Giannozzi, P.; et al. Advanced Capabilities for Materials Modelling with Quantum Espresso. *J. Phys. Condens. Matter* **2017**, *29*, 465901.
(27) Zhang, Y.-H.; Chen, Y.-B.; Zhou, K.-G.; Liu, C.-H.; Zeng, J.; Zhang, H.-L.; Peng, Y. Improving Gas Sensing Properties of Graphene by Introducing Dopants and Defects: A First-Principles Study. *Nanotechnology* **2009**, *20*, 185504.
(28) Mehdi Aghaei, S.; Monshi, M. M.; Torres, I.; Zeidi, S. M. J.; Calizo, I. Dft Study of Adsorption Behavior of No, Co, No2, and Nh3 Molecules on Graphene-Like Bc3: A Search for Highly Sensitive Molecular Sensor. *Appl. Surf. Sci.* **2018**, *427*, 326−333.
(29) Momma, K.; Izumi, F. Vesta 3 for Three-Dimensional Visualization of Crystal, Volumetric and Morphology Data. *J. Appl. Crystallogr.* **2011**, *44*, 1272−1276.
(30) Li, B.; Ou, P.; Wei, Y.; Zhang, X.; Song, J. Polycyclic Aromatic Hydrocarbons Adsorption onto Graphene: A Dft and Aimd Study. *Materials* **2018**, *11*, 726.
(31) Sarkar, S.; Bekyarova, E.; Niyogi, S.; Haddon, R. C. Diels-Alder Chemistry of Graphite and Graphene: Graphene as Diene and Dienophile. *J. Am. Chem. Soc.* **2011**, *133*, 3324−3327.
(32) Brisebois, P. P.; Kuss, C.; Schougaard, S. B.; Izquierdo, R.; Siaj, M. New Insights into the Diels-Alder Reaction of Graphene Oxide. *Chemistry* **2016**, *22*, 5849−5852.
(33) Riccardi, D.; Guo, H.-B.; Parks, J. M.; Gu, B.; Summers, A. O.; Miller, S. M.; Liang, L.; Smith, J. C. Why Mercury Prefers Soft Ligands. *J. Phys. Chem. Lett.* **2013**, *4*, 2317−2322.
(34) Yoder, C. H. Appendix 3: Metallic, Covalent, and Ionic Radii. *Ionic Compounds: Applications of Chemistry and Mineralogy*; John Wiley & Sons Ltd.: New Jersey, 2006; p 171.
(35) Bala, T.; Prasad, B. L. V.; Sastry, M.; Kahaly, M. U.; Waghmare, U. V. Interaction of Different Metal Ions with Carboxylic Acid Group: A Quantitative Study. *J. Phys. Chem. A* **2007**, *111*, 6183−6190.
(36) Speight, J. G. *Lange's Handbook of Chemistry*, 17th ed.; McGraw-Hill Education: New York, 2017; p 1293.
(37) Usepa Clean Water Act. https://www.govinfo.gov/content/pkg/USCODE-2018-title33/pdf/USCODE-2018-title33-chap26.pdf (accessed Oct 22, 2021).
(38) Shtepliuk, I.; Vagin, M.; Ivanov, I. G.; Iakimov, T.; Yazdi, G. R.; Yakimova, R. Lead (Pb) Interfacing with Epitaxial Graphene. *Phys. Chem. Chem. Phys.* **2018**, *20*, 17105−17116.
(39) Liu, W.; Zeng, J.; Gao, Y.; Li, H.; Rooij, N. F. d.; Umar, A.; Algarni, H.; Wang, Y.; Zhou, G. Charge Transfer Driven by Redox Dye Molecules on Graphene Nanosheets for Room-Temperature Gas Sensing. *Nanoscale* **2021**, *13*, 18596.

https://doi.org/10.1021/acs.jpcc.1c07247
J. Phys. Chem. C 2021, 125, 26418−26428